Chinese Chemical Letters 32 (2021) 842–848

Contents lists available at ScienceDirect

Chinese Chemical Letters

journal homepage: www.elsevier.com/locate/cclet

Communication

Facile synthesis of metal-polyphenol-formaldehyde coordination polymer colloidal nanoparticles with sub-50 nm for T_1-weighted magnetic resonance imaging

Jing Qin[a,1], Guohai Liang[b,1], Bingxi Feng[a], Gen Wang[a], Na Wu[a], Yonghui Deng[c], Ahmed A. Elzatahry[d], Abdulaziz Alghamdi[e], Yongxi Zhao[a], Jing Wei[a,*]

[a] *The Key Laboratory of Biomedical Information Engineering of Ministry of Education, School of Life Science and Technology, Xi'an Jiaotong University, Xi'an 710049, China*
[b] *College of Biophotonics, South China Normal University, Guangzhou 510631, China*
[c] *Department of Chemistry, Fudan University, Shanghai 200433, China*
[d] *Materials Science and Technology Program, College of Arts and Sciences, Qatar University, PO Box 2713, Doha, Qatar*
[e] *Department of Chemistry, College of Science, King Saud University, P.O. Box 2455, Riyadh 11451, Saudi Arabia*

ARTICLE INFO

Article history:
Received 17 April 2020
Received in revised form 14 May 2020
Accepted 18 May 2020
Available online 21 May 2020

Keywords:
Coordination polymer
Nanoparticle
Self-assembly
Plant polyphenol
Contrast agent

ABSTRACT

Plant polyphenol-based coordination polymers (CPs) with ultra-small particle size and tailorable compositions are highly desired in biomedical applications, but their synthesis is still challenging due to the sophisticated coordination assembly process and unavoidable self-oxidation polymerization of polyphenol. Herein, a general ligand covalent-modification mediated coordination assembly strategy is proposed for the synthesis of water-dispersible CPs with tunable metal species (*e.g.*, Gd, Cu, Ni, Zn, Fe) and ultra-small diameter (8.6–37.8 nm) using nontoxic plant polyphenol (*e.g.*, tannic acid, gallic acid) as a polymerizable ligand. Polyphenol molecules react with formaldehyde firstly, which can effectively retard the oxidation induced self-polymerization of polyphenol and lead to the formation of metal ions containing CPs colloidal nanoparticles. These ultrafine nanoparticles with stably chelated metal ions are highly water dispersible and thus advantageous for bioimaging. As an example, ultra-small Gd contained CPs exhibit higher longitudinal relaxivity ($r_1 = 25.5$ L mmol^{-1} s^{-1}) value with low r_2/r_1 (1.19) than clinically used Magnevist (Gd-DTPA, $r_1 = 3.7$ L mmol^{-1} s^{-1}). Due to the enhanced permeability and retention effect, they can be further used as a positive contrast agent for T_1-weighted MR imaging of tumour.

Nanoscale coordination polymers (CPs) with tailorable organic ligands and metal species, various morphologies and structures, as well as tunable particle size, have attracted increasing attentions due to their broad applications such as sensing, biomedical imaging and therapy [1–7]. Metal-phenolic coordination polymers (MPCPs) or metal-phenolic networks (MPNs) are one kind of CPs, which are usually constructed using plant polyphenol as a build block [8–17]. Plant polyphenols are secondary metabolites of plant with highly diverse chemical structures, which are widely existed in fruits and vegetables. Specially, plant polyphenols show antifouling, antibacterial, antioxidant, nontoxic and adhesive properties, as well as strong chelate abilities with various metal ions including rare earth, transitional and alkaline earth metal ions [18–36]. Based on the coordination assembly, the resultant MPCPs with different metal species show fascinating optical and magnetic properties, as well as broad applications in catalysis, separation, medical imaging, sensing and drug delivery [18–36]. In order to fully explore their potential applications and improve their performance, it is desirable to develop a versatile synthesis strategy to realize the controllable synthesis of MPCPs with tunable compositions and nanostructures.

Particle size is one of the most important parameters for CPs, which plays a pivotal role in determining their behavior *in vivo* involving cellular internalization, biodistribution, clearance rate and excretion pathway [37]. For gadolinium-based coordination polymer nanoparticles, the smaller size leads to higher contrast ability due to larger specific surface area, while smaller size results

* Corresponding author.
E-mail address: jingwei@xjtu.edu.cn (J. Wei).
[1] These authors contributed equally to this work.

https://doi.org/10.1016/j.cclet.2020.05.021
1001-8417/

in lower chemical stability and the higher risk of leakage of toxic gadolinium ion [38–42]. Generally, MPCP particles were synthesized *via* the template synthesis strategy. A sacrificed template such as polystyrene sphere was usually used [10]. Due to the strong adhesive property of polyphenol, the metal ions and polyphenolic ligands were deposited on the surface of template. After selective removal of template, MPCP capsules were obtained. The diameter of the capsules was relied on the size of template. Generally, it is difficult to synthesize MPCPs with diameter below 50 nm due to the limited choice of template and the complicated procedures for selective removal of the template. Alternatively, template-free synthesis strategy did not require external template or the tedious procedures for selective removal of template. The nanoscale MPCPs can be synthesized using different synthesis strategies such as self-assembly *via* coordination or hydrogen bonding interactions and sol-gel process [43–50]. During the synthesis process, a competitive ligand was used to modulate the coordination assembly process. For example, poly(vinylpyrrolidone) (PVP) can effectively control the particle size of CPs [2]. Liu *et al.* reported the synthesis of coordination polymer nanodots with a small diameter of 5.3 nm and excellent renal clearance properties based on the coordination reactions among Fe ions, gallic acid and PVP [51]. In our previous work, a controllable sol-gel synthesis strategy was proposed for the preparation of MPCP colloidal spheres with diameter of around 300 nm [44]. Despite great successes in the synthesis of MPCP particles, the size control for MPCP in the sub 50 nm scale is still a great challenge. The small diameter can effectively enhance the dispersion and stability of MPCP nanoparticles when they are in the buffer solution. Moreover, the smaller nanoparticles show larger surface-to-volume ratio and higher r_1, which are beneficial for *in vivo* T_1-weighted MR imaging. Moreover, most of the previous reports mainly focused on iron-phenolic coordination polymers. The controllable synthesis and *in vivo* biomedical applications for other metal-phenolic coordination polymer nanoparticles have rarely been investigated. To the best of our knowledge, the synthesis of MPCPs with ultra-small diameter (10−50 nm) and tunable metal species have rarely been reported due to the difficulty to mediate the metal-ligand coordination assembly process in the molecular scale.

Herein, we demonstrate a general ligand covalent-modification mediated coordination assembly strategy for the synthesis of nanoscale MPCPs with ultra-small hydrodynamic diameter (8.6–37.8 nm), high colloidal stability and tunable metal species (*e.g.*, Gd, Cu, Ni, Zn and Fe) using plant polyphenol as an organic ligand. The polyphenolic ligand (*i.e.*, tannic acid, abbreviation as TA) is firstly modified *via* a phenol-formaldehyde reaction, which can effectively retard the oxidation induced self-polymerization of polyphenol in alkaline conditions. After adding different metal ions, various MPCP nanoparticles are successfully synthesized *via* the metal-ligand coordination assembly process. PVP can effectively prevent the aggregation of MPCP nanoparticles by capping on the surface of MPCP nanoparticles. Moreover, other polyphenols such as gallic acid (GA) can also be used as a ligand to synthesize MPCP nanoparticles. To explore their potential biomedical application, Gd containing CPs (*i.e.*, Gd-TA), which show high colloidal stability, low cytotoxicity and leakage of Gd ions, high longitudinal relaxivity (r_1 = 25.5 L mmol^{-1} s^{-1}) value with low r_2/r_1 (1.19), are successfully used as a positive contrast agent for T_1-weighted MR imaging of the tumour.

The synthesis of nanoscale MPCPs mainly included two steps (Fig. 1). Firstly, polyphenol (*e.g.*, TA) reacted with formaldehyde in the alkaline conditions to form TA-formaldehyde oligomer. Secondly, different metal ions were added to trigger the metal-ligand coordination assembly. In this process, PVP molecules were used to prevent the aggregation of MPCP nanoparticles. As a result, MPCP nanoparticles with small diameter and high colloidal stability were successfully synthesized. The obtained samples were denoted M-TA (M refers metal species). Here, Gd-TA CPs were used as a typical example. The photograph of Gd-TA in water (1.0 mg/mL) showed a clear solution, indicating a good dispersibility (Fig. 2a). After standing for 30 days, no precipitate was observed, revealing a high colloidal stability of Gd-TA in water. Transmission electron microscopy (TEM) image of Gd-TA showed spherical nanoparticles with an average size of 20.2 nm (Fig. 2b and Fig. S1 in Supporting information). Gd-TA CPs were further characterized by atomic force microscopy (AFM) (Fig. 2c). The diameters of Gd-TA CPs labeled in the AFM image were 16.9, 9.8 and 12.7 nm respectively by calculation of the height of nanoparticles (Fig. 2d). The hydrodynamic diameter of Gd-TA was centered at 21.0 nm (Fig. 2e), which remained nearly unchanged (20.9 nm) after storage for one month. When Gd-TA CPs were transferred to other buffers, such as HEPES (pH 7.4, 0.01 mol/L), Tris-Borate-EDTA (TBE) (pH 8.0, 1x), phosphate-buffered saline (pH 7.3, 0.01 mol/L), NaCl solution (0.9 wt%) or dulbecco's modified eagle medium (DMEM) supplemented with 10% foetal bovine serum (FBS) (v/v), Gd-TA CPs still showed good dispersibility

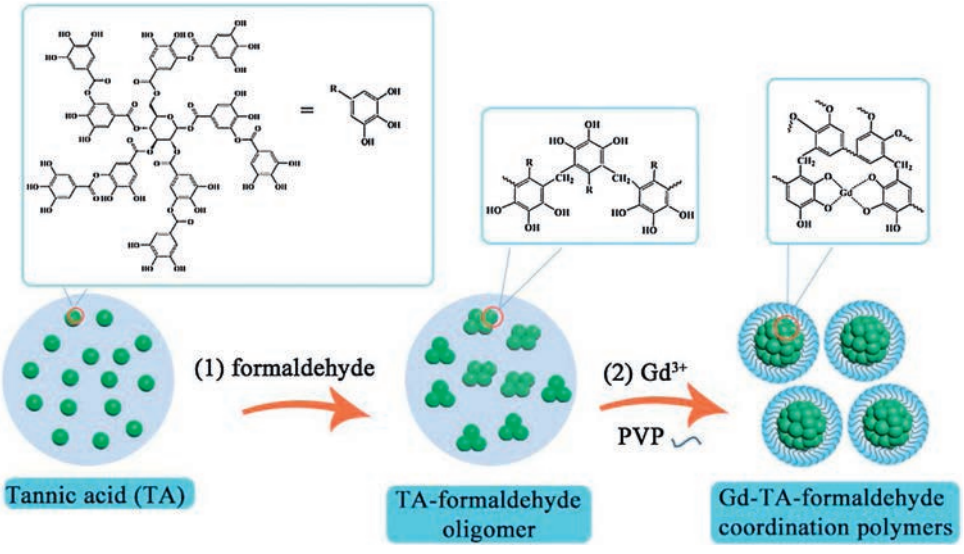

Fig. 1. Schematic illustration of the synthesis of ultra-small Gd-TA-formaldehyde coordination polymer nanoparticles.

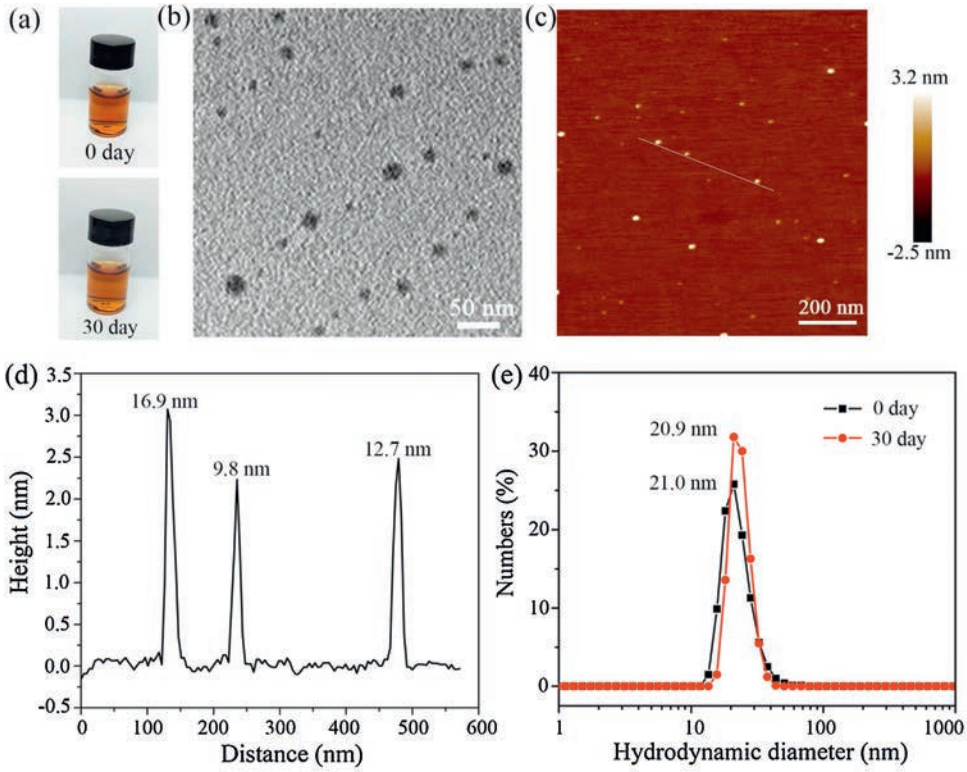

Fig. 2. (a) Photographs for Gd-TA solution for 0 and 30 days. (b) TEM and (c) AFM images for Gd-TA nanoparticles. (d) The height profile along the line marked in the AFM image. (e) The hydrodynamic diameter distributions of Gd-TA solution at 0 day and 30 days measured by DLS.

without macroscopic aggregations (Fig. S2 in Supporting information). The hydrodynamic diameters of Gd-TA CPs in these buffers were in the range from 18.1 nm to 21.1 nm, which were close to 21.0 nm (the diameter in water). Such excellent dispersibility would facilitate their further biomedical applications.

X-ray diffraction (XRD) patterns for Gd-TA nanoparticles revealed an amorphous structure (Fig. S3 in Supporting information). X-ray photoelectron spectroscopy (XPS) for Gd-TA showed the existence of C, N, O and Gd element (Fig. S4 in Supporting information). Gd 4d spectra showed two peaks centered at 142.1 and 148.0 eV, which were ascribed to the Gd $4d_{5/2}$ and Gd $4d_{3/2}$, respectively [52]. Gd 3d spectra showed two peaks centered at 1187.1 and 1221.0 eV, which were ascribed to the Gd $3d_{5/2}$ and Gd $3d_{3/2}$, respectively. The N 1s spectra can be fitted with two peaks at about 398.49 and 399.24 eV, which are assigned to pyridinic nitrogen and pyrrolic nitrogen, respectively [53]. The nitrogen atoms in the CPs were from PVP and ammonia. The presence of pyrrolic nitrogen atoms indicated the existence of PVP on the surface of Gd-TA. Gd contents were determined by inductively coupled plasma-mass spectrometry (ICP-MS). The Gd contents in the Gd-TA were 2.97%, 4.30%, 5.52%, 6.67% and 7.42 wt% when the mass ratios of Gd precursor to TA were 0.125, 0.25, 0.375, 0.5 and 0.626 respectively (Fig. S5a in Supporting information). The Gd contents in Gd-TA showed a linear relationship with the mass ratio of Gd source to TA. The hydrodynamic diameter of Gd-TA nanoparticles increased from 8.6 nm to 26.6 nm when the mass ratios of Gd precursor to TA increased from 12.5 wt% to 62.5 wt% (Fig. S5b in Supporting information). Such results indicated that the size of Gd-TA CPs could be slightly adjusted by changing the amount of Gd precursor. With more amounts of Gd precursors added, more Gd ions would coordinate with the TA molecules (or oligomers) and then the size of the resultant CPs increased.

In order to investigate the possible formation mechanism of the ultra-small coordination polymer nanoparticles, we firstly studied the recipes during the synthesis process. Gd ions could coordinate with TA directly in alkaline conditions. When neither PVP nor formaldehyde was used, fibrous Gd-TA CPs with size in the micrometer scale were obtained (Fig. S6a in Supporting information). XRD patterns of the Gd-TA fiber showed highly crystalline framework (Fig. S3 in Supporting information). When PVP was used and formaldehyde was not used, Gd-TA rhombohedron was prepared (Fig. S6b in Supporting information). XRD patterns of the Gd-TA rhombohedron also showed a crystalline framework (Fig. S3), which were consistent to that of the Gd-TA fiber. PVP molecule has amide moieties, which can weakly coordinate with Gd ions. Consequently, the nucleation and growth process of Gd-TA coordination crystals can be mediated by PVP molecules. As a result, Gd-TA CPs showed different morphologies and small diameters after addition of PVP. However, PVP cannot affect the crystalline structure of CPs, indicating that PVP only acted as a protective layer to mediate the growth of Gd-TA crystals. When formaldehyde was used and PVP was not used, Gd-TA nanoparticles with diameter below 50 nm were obtained (Fig. S6c in Supporting information). XRD patterns of Gd-TA nanoparticles showed an amorphous structure (Fig. S3 in Supporting information), indicating that formaldehyde could effectively prevent the crystallization process of Gd-TA CPs.

Because both formaldehyde and PVP can effectively change the morphology, size and crystalline structure of Gd-TA CPs in different ways, we further changed the amount of formaldehyde or PVP to investigate the structure evolution of Gd-TA CPs. When the volume of formaldehyde increased from 0 to 3.8 mL, the hydrodynamic diameters of the obtained Gd-TA deceased from 287.1–18.8 nm (Fig. 3a). When the amount of PVP increased, the hydrodynamic diameters of Gd-TA decreased from 375.9–22.7 nm (Fig. 3b). We further measured the Zeta potential of Gd-TA nanoparticles

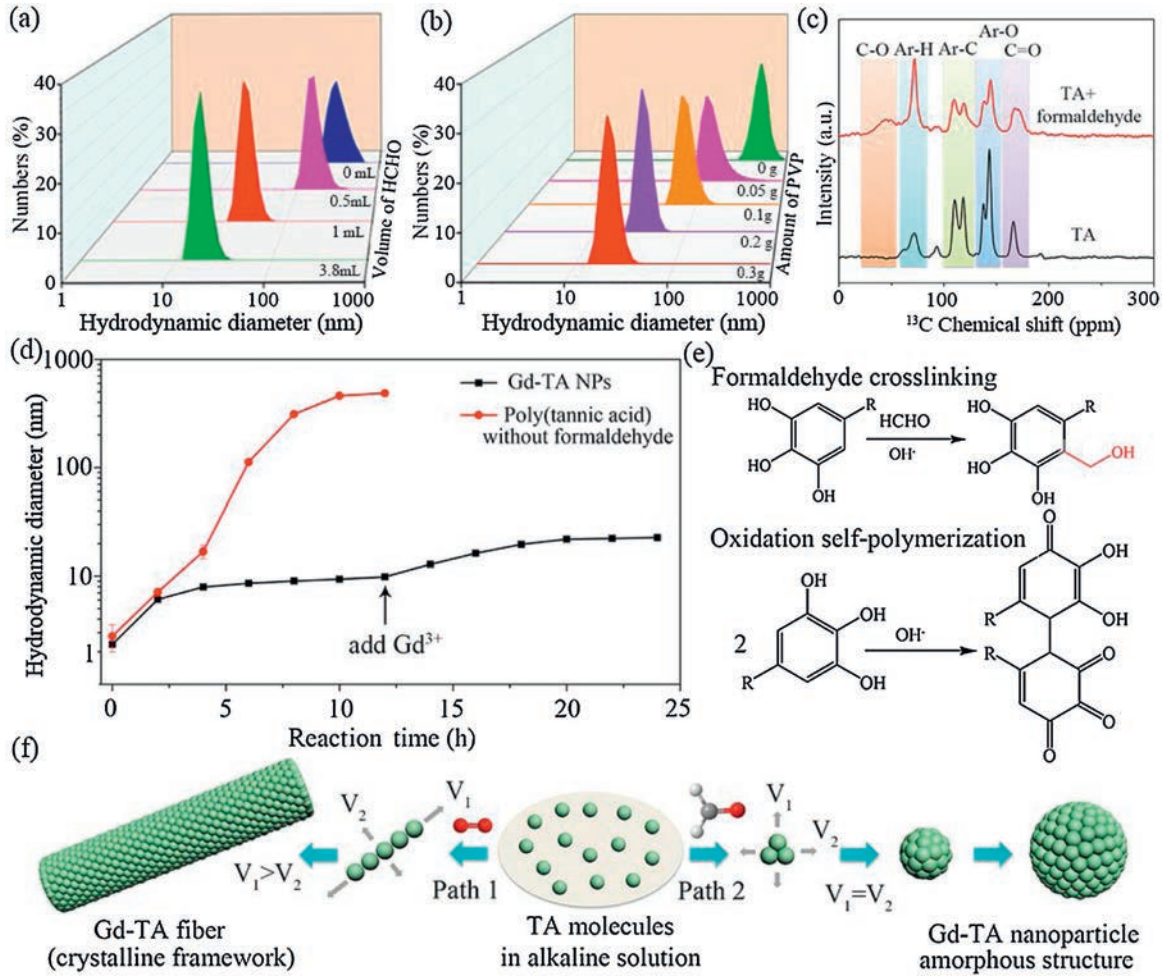

Fig. 3. (a) The hydrodynamic diameter for Gd-TA synthesized with different amounts of formaldehyde. (b) The hydrodynamic diameter for Gd-TA coordination polymers synthesized using different amounts of PVP. (c) ^{13}C NMR spectra for TA and TA oligomer. (d) The hydrodynamic diameter for TA-based nanoparticles at different reaction times. (e) The possible polymerization reaction of TA in alkaline conditions. (f) The proposed formation mechanism of TA-based nanomaterials *via* two different assembly paths.

synthesized using different amounts of PVP (Fig. S7 in Supporting information). When the amount of PVP increased from 0 to 0.4 g, the Zeta potential increased from −16.1 mV to −0.86 mV. Gd-TA CPs showed negatively charged surface. PVP showed neutral surface. When the amount of PVP increased, more PVP molecules were capped on the surface of Gd-TA nanoparticles, resulting into a decreased Zeta potential. The hydrodynamic diameters of CPs were further monitored during the synthesis process. At the first stage, the hydrodynamic diameter was around 2 nm, which could be ascribed to the TA molecules (Fig. 3d). When formaldehyde was added into the solution, the diameter slightly increased to 6 nm. Solid-state nuclear magnetic resonance (NMR) was further employed to characterize the reaction between TA and formaldehyde (Fig. 3c). Solid-state ^{13}C NMR for TA molecule showed four bands, which could be ascribed to C=O, Ar-O, Ar-C and Ar-H. After addition of formaldehyde, an obvious new peak at around 50 ppm was observed. The new peak could be attributed to the formation of Ar-C-O band, indicating a phenol-formaldehyde addition reaction between TA and formaldehyde in the alkaline conditions. The diameter of oligomers was stable from 6 to 10 h, indicating that further polymerization of TA was suppressed. When Gd ions were added into the solution, the diameter was slightly increased to 20 nm. The Gd ions can further crosslink the TA-formaldehyde oligomers *via* a metal-catechol coordination assembly process. The diameter kept nearly constant after 20 h. For comparison, the hydrodynamic diameters of polymers in the absence of formaldehyde were further investigated (Fig. 3d). The diameter increased gradually from 2 nm to 486 nm when the reaction time reached 12 h. Solid-state NMR results showed an obvious shift of bands for poly(tannic acid) when compared with that of tannic acid (Fig. S8 in Supporting information). In alkaline condition, TA molecules can be spontaneously oxidized by oxygen, triggering an oxidization polymerization process of TA. As a result, fibrous MPCPs were obtained.

Based on the above results, we speculate that ultra-small coordination polymer nanoparticles were formed *via* a ligand covalent-modification mediated coordination assembly process. In alkaline conditions, polyphenol not only shows strong chelate ability towards different metal ions, but also can be polymerized *via* oxidation induced polymerization process [54]. Because the coordination reaction shows faster kinetics than the oxidation induced polymerization reaction, the formation of MPCPs is mainly driven by the coordination assembly process (Fig. S9 in Supporting information). However, when the synthesis target was the nanoscale CPs with ultra-small particle size, the coordination assembly process should be conducted in a controlled manner. In this situation, the oxidation induced polymerization of polyphenol cannot be ignored, which also obviously affect the particle size of nanoscale CPs. In the previous report, tannin gel was synthesized by covalent crosslinking of tannin with formaldehyde [55,56].

Herein, it was found that the covalent crosslinking of TA with formaldehyde can effectively retard the oxidation induced self-polymerization of TA (Fig. 3e). In the alkaline condition, TA can be oxidized and polymerized to form polymer crystals. The growth rate of crystals in each direction was different (Fig. 3f). As a result, the fibrous polymer crystals were obtained. The addition of metal species may not obviously affect the fibrous morphology according to our previous report [25]. As a result, fibrous MPCPs with large crystal size were prone to be formed *via* this growth pathway. When PVP molecules were utilized to mediate the growth process of crystals, rhombohedron crystals with a few hundreds of nanometers were obtained. However, the covalent modification of polyphenol ligand using formaldehyde would change the pathway of the polymerization process. As a result, nanoparticles with small size and amorphous framework were obtained. When metal ions were added into the solution, metal-phenolic coordination polymers were formed due to the metal-ligand coordination assembly process. The metal ions not only coordinate with polyphenol to form metal-phenolic coordination polymers, but also induce the aggregation of nanoparticles by connecting adjacent particles *via* a coordination bond. PVP molecules can modulate the metal-polyphenol coordination assembly process by weakly coordinating with metal ions. When sufficient amount of PVP was used, PVP can effectively prevent the aggregation of the nanoparticles by capping on the surface of CPs.

In order to verify the universality of the proposed strategy, different kinds of metal ions, polyphenols, aldehydes or PVP molecules with different molecular weights were used during the synthesis process. Metal-phenolic coordination polymer nanoparticles with ultra-small diameters were also successfully synthesized. For example, when $Cu(NO_3)_2$, $Ni(NO_3)_2$, $Zn(NO_3)_2$ and $FeSO_4$ were used as a metal precursor, Cu-TA, Ni-TA, Zn-TA and Fe-TA nanoparticles were successfully synthesized. The hydrodynamic diameters of Cu-TA, Ni-TA, Zn-TA and Fe-TA were 23.7, 37.8, 19.0 and 18.1 nm respectively (Fig. S10a in Supporting information). The MPCP nanoparticles were formed by the coordination assembly process. The differences in the diameter for different MPCPs were due to different coordination interactions between metal species and polyphenol ligand. Such nanoparticles can be easily dispersed in water like Gd-TA (Fig. S11 in Supporting information). TEM images further confirmed the spherical morphology and uniform diameter (Figs. S10b-e in Supporting information). When other aldehydes such as glutaraldehyde and acetaldehyde were used to replace formaldehyde, Gd-TA nanoparticles with hydrodynamic diameters of 15.7 and 18.2 nm were synthesized respectively (Fig. S12a in Supporting information). The diameter of the particles was slightly smaller than that of Gd-TA synthesized using formaldehyde. When PVP with different molecular weight (24 kg/mol) was used, the hydrodynamic diameter of Gd-TA was 15.9 nm (Fig. S12b in Supporting information). When other polyphenols such as gallic acid (GA) were used as the organic ligands, gadolinium-phenolic coordination polymer nanoparticles (Gd-GA) with hydrodynamic diameters of 32.7 nm were prepared (Fig. S12c in Supporting information). Such results further proved that this versatile synthesis strategy could be used to synthesize coordination polymers with ultra-small diameter (< 50 nm) and tailorable compositions.

Encouraged by the high colloidal stability and ultra-small particle size of MPCPs, we further investigated their potential biomedical applications. Specially, Gd-TA nanoparticles were used as a contrast agent for magnetic resonance imaging (MRI). The cytotoxicity of Gd-TA was firstly evaluated on Hela, U87 and MCF-7 cells by a standard 3-(4,5-dimethylthiazol-2-yl)-2,5-diphenyltetrazolium bromide (MTT) method (Fig. S13 in Supporting information). The viability of all three cells was not significantly affected when the concentration of Gd-TA CPs reached 960 μg/mL. Such results indicate that Gd-TA CPs have a low cytotoxicity.

One of the main issues for Gd-based CPs was the leakage of toxic Gd ions owing to the small diameter of CPs and their unstable framework. The stability of Gd-TA was investigated by dialysis against PBS buffer (Fig. S14a in Supporting information). The residual Gd in Gd-TA CPs was as high as 99.0% after dialysis for 168 h. Comparably, the residual Gd in the crystalline Gd-TA rhombohedron obtained without usage of formaldehyde was only 61.9% after dialysis for 168 h. These results indicate that the formaldehyde can effectively improve the stability of the Gd-TA coordination polymers. Formaldehyde can crosslink the polyphenol ligand, resulting into a more rigid and dense framework of the coordination polymers (Fig. S14b in Supporting information). These results also indicate that covalent crosslinking of organic ligand in the coordination polymers can effectively increase the stability of coordination polymers. Because free Gd ions are toxic, such excellent stability of Gd-TA CPs is beneficial for their application in MRI.

Inspired by the above results, we further studied the relaxivity of the Gd-TA CPs. The longitudinal (r_1) and transverse (r_2) relaxivities of the Gd-TA NPs were 25.5 and 30.3 L $mmol^{-1}$ s^{-1} respectively (Fig. 4a). The r_2/r_1 value was 1.19, suggesting that Gd-TA CPs could be employed as an efficient contrast agent for T_1-weighted MRI. The r_1 value was 6.9 folds higher than that of Magnevist (Gd-DTPA, r_1 = 3.7 L $mmol^{-1}$ s^{-1}) measured in the same conditions, and was also higher than the previously reported gadolinium-phenolic coordination polymers (Table S1 in Supporting information) [23,43,51]. This high r_1 value may be ascribed to: (1) the small size of the particles, which facilitate the approaching of water molecules to the metal sites; (2) PVP coating, which slows down the rotational diffusion of the particles, resulting into increased relaxivity at low field strengths [57,58]. To further evaluate the MRI contrasting ability, T_1-weighted MR images of Gd-TA dispersions with different Gd concentrations were collected using a 1.0 T MRI scanner (Fig. 4c). The intensity of MR signal was positively correlated with the concentrations of Gd in the solution. Gd-TA CPs showed a higher signal intensity than Gd-DTPA at the same Gd concentrations.

To further evaluate the MRI performance *in vivo*, EMT-6 tumour bearing mice were injected with Gd-TA CPs solution (4 mg/kg) *via* the tail veins and placed in a 1.0 T MRI scanner. The MRI signal of the tumour increased gradually, and reached a maximum at 2 h post-injection, indicating the effective uptake of Gd-TA CPs in the tumour *via* the enhanced permeability and retention (EPR) effect (Figs. 4b and d). The highest relative signal enhancement (RSE) was 77.8%±7.1%. Subsequently, the MR signals receded slowly. Such results further revealed that Gd-TA CPs can be used as an efficient MRI contrast agent for enhancing the contrast of the tumour region.

It is crucial for an ideal MRI contrast agent to safely metabolize in biological systems. Here the biodistribution and clearance pathway of Gd-TA CPs *in vivo* were investigated by MRI. The mice were intravenously injected with Gd-TA CPs solution (4 mg/kg) and the MR images were acquired at 0, 0.25, 0.5, 1, 2, 4, 6 and 12 h after injection (Figs. S15a and b in Supporting information). The MRI signals enhanced in the veins and the RSE reached 31.2%±2.3% at 2 h post-injection. The liver region showed the maximum RSE (25.3%±2.4%) at 2 h after intravenous injection, suggesting that Gd-TA CPs were mainly accumulated in the reticuloendothelial system. After 12 h, the signal in liver region obviously reduced, indicating that most of Gd-TA could be effectively excreted out of mice body by hepatobiliary pathway [59,60]. However, the MRI signal in the kidney and bladder enhanced slightly throughout the whole experiment, indicating that only a small portion of Gd-TA CPs were excreted from the body *via* renal filtration.

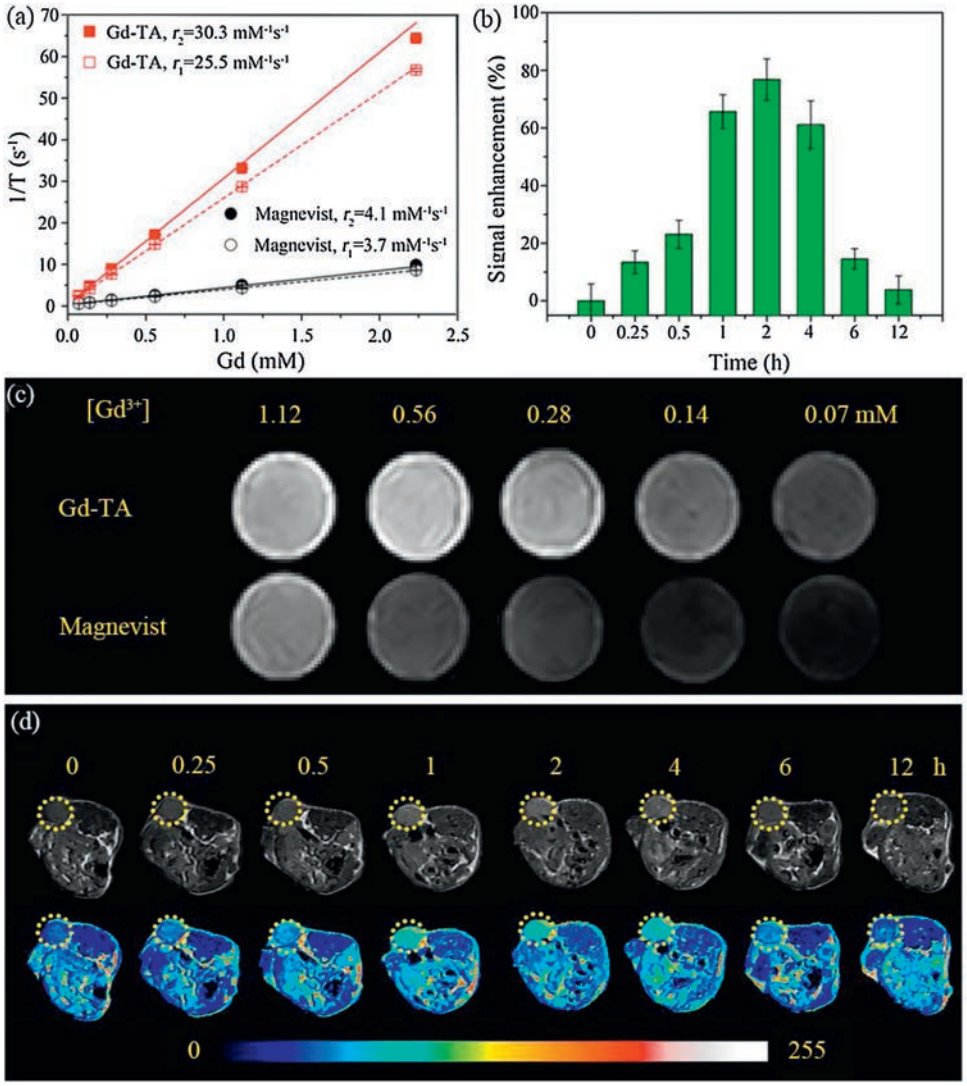

Fig. 4. (a) Plot of $1/T_1$ and $1/T_2$ over Gd concentration of Gd-TA nanoparticles and Magnevist (Gd-DTPA). (b) The quantification of signal enhancement for tumours after intravenous injection of Gd-TA at different time intervals. (c) MR images of Gd-TA nanoparticles and Magnevist (Gd-DTPA) with different concentrations of Gd. (d) *In vivo* T_1-weighted MR images of nude mice bearing tumours after intravenous injection of Gd-TA at different time intervals.

Additionally, the feces and urine of mice were collected after intravenous injection of Gd-TA CPs for MRI and ICP-MS analysis. After intravenous injection for 60 h, the accumulation of Gd in fecal and urinary excretion were 64.2% and 18.7% of the injected dose respectively (Fig. S15c in Supporting information). This results further confirmed that hepatobiliary pathway was the main metabolic pathway of Gd-TA in mice body. Correspondingly, MRI signal of the feces enhanced continuously from 12 h to 60 h. These results proved that Gd-TA CPs could be effectively excreted out of mice body, which was beneficial to minimize long-term retention and potential toxicity of the particles.

Furthermore, we systematically evaluated the *in vivo* toxicity of Gd-TA through hematology and histochemical analyses. Consistent with the control group, the hematology analysis parameters of Gd-TA-treated groups at 1 and 3 days were in good agreement with the reference normal ranges (Fig. S16 in Supporting information) [61]. The major organs (spleen, lung, heart, liver and kidneys) of the Gd-TA-treated group were collected at 1 and 3 days after injection for a histology analysis. There were not any noticeable abnormalities or lesions in the major organs between the control group and the treatment group (Fig. S17 in Supporting information). The above results further confirmed the low toxicity of the Gd-TA. The preliminary toxicity analysis *in vivo* revealed that Gd-TA may be used as a potential nanoplatform for MRI.

In summary, coordination polymer colloidal nanoparticles with ultra-small diameters (8.6–37.8 nm) and tunable metal species (*e.g.*, Gd, Cu, Ni, Zn, Fe) were successfully synthesized *via* a ligand covalent-modification-mediated coordination assembly strategy using plant polyphenol as a polymerizable ligand. Formaldehyde can effectively adjust the coordination assembly process by reacting with polyphenolic ligand *via* a phenol-formaldehyde addition reaction. As a result, instead of fibrous coordination polymer crystals, amorphous metal-polyphenol coordination nanoparticles with ultra-small size and high colloidal stability were obtained. Moreover, the covalent modification of polyphenolic ligand can effectively increase the stability of coordination polymers (Gd-TA), resulting into a low leakage of Gd ions. Gd-TA CPs showed high longitudinal relaxivity (r_1 = 25.5 L mmol^{-1} s^{-1}) with a low r_2/r_1 ratio (1.19), which were used as a promising contrast agent for enhanced T_1-weighted MRI of the tumour region of mice. We believe that the general synthesis strategy reported here can be applied for the synthesis of multifunctional polymer

nanoparticles using renewable and nontoxic plant polyphenol as a ligand for various biomedical application purposes, such as sensing, imaging and therapy.

Declaration of competing interest

The authors declare that they have no known competing financial interests or personal relationships that could have appeared to influence the work reported in this paper.

Acknowledgments

This work was financially supported by the National Natural Science Foundation of China (Nos. 21701130 and 311343), the Fundamental Research Funds for the Central Universities, and "Young Talent Support Plan" of Xi'an Jiaotong University. We thank Miss Jiao Li, Mr Zijun Ren at Instrument Analysis Center of Xi'an Jiaotong University for their assistance with TEM and SEM analysis. The authors extend their thanks to Research Supporting Project number (No. RSP-2019/155), King Saud University, Riyadh, Saudi Arabia.

Appendix A. Supplementary data

Supplementary material related to this article can be found, in the online version, at doi:https://doi.org/10.1016/j.cclet.2020.05.021.

References

[1] S. Rojas, A. Arenas-Vivo, P. Horcajada, Coord. Chem. Rev. 388 (2019) 202–226.
[2] S. Wang, C.M. McGuirk, A. d'Aquino, J.A. Mason, C.A. Mirkin, Adv. Mater. 30 (2018) 1800202.
[3] L. Wang, M. Zheng, Z. Xie, J. Mater. Chem. B 6 (2018) 707–717.
[4] T. Simon-Yarza, A. Mielcarek, P. Couvreur, C. Serre, Adv. Mater. 30 (2018) 1707365.
[5] K. Lu, T. Aung, N. Guo, R. Weichselbaum, W. Lin, Adv. Mater. 30 (2018) 1707634.
[6] M. Wu, Y. Yang, Adv. Mater. 29 (2017) 1606134.
[7] M. Gimenez-Marques, T. Hidalgo, C. Serre, P. Horcajada, Chem. Rev. 307 (2016) 342–360.
[8] M.A. Rahim, S.L. Kristufek, S. Pan, J.J. Richardson, F. Caruso, Angew. Chem. Int. Ed. 58 (2019) 1904–1927.
[9] H. Ejima, J.J. Richardson, F. Caruso, Nano Today 12 (2017) 136–148.
[10] J. Guo, Y. Ping, H. Ejima, et al., Angew. Chem. Int. Ed. 53 (2014) 5546–5551.
[11] P. Zhang, L. Wang, S. Yang, et al., Nat. Commun. 8 (2017) 15020.
[12] J. Wei, Y. Liang, Y. Hu, et al., Angew. Chem. Int. Ed. 55 (2016) 12470–12474.
[13] J. Wei, Y. Liang, Y. Hu, et al., Angew. Chem. Int. Ed. 55 (2016) 1355–1359.
[14] J. Guo, B.L. Tardy, A.J. Christofferson, et al., Nat. Nanotechnol. 11 (2016) 1105–1111.
[15] P. Zhang, H. Li, G.M. Veith, S. Dai, Adv. Mater. 27 (2015) 234–239.
[16] K. Kim, M. Shin, M.Y. Koh, et al., Adv. Funct. Mater. 25 (2015) 2402–2410.
[17] H. Ejima, J.J. Richardson, K. Liang, et al., Science 341 (2013) 154–157.
[18] L.Q. Xu, K.G. Neoh, E.T. Kang, Prog. Polym. Sci. 87 (2018) 165–196.
[19] W. Zhu, J. Guo, Y. Ju, et al., Adv. Mater. 31 (2019) 1806774.
[20] J. Cui, K. Alt, Y. Ju, et al., Biomacromolecules 20 (2019) 3592–3600.
[21] G. Yun, J.J. Richardson, M. Biviano, F. Caruso, ACS Appl. Mater. Interfaces 11 (2019) 6404–6410.
[22] A. Shavandi, A.E.D.A. Bekhit, P. Saeedi, et al., Biomaterials 167 (2018) 91–106.
[23] T. Liu, M. Zhang, W. Liu, et al., ACS Nano 12 (2018) 3917–3927.
[24] G. Wang, J. Qin, X. Zhou, et al., Adv. Funct. Mater. 28 (2018) 1806144.
[25] H.B. Huang, J. Qin, G. Wang, et al., CrystEngComm 20 (2018) 7626–7630.
[26] R. Riccò, W. Liang, S. Li, et al., ACS Nano 12 (2018) 13–23.
[27] Q. Dai, H. Geng, Q. Yu, J. Hao, J. Cui, Theranostics 9 (2019) 3170–3190.
[28] Z. Jia, Y. Zeng, P. Tang, et al., Chem. Mater. 31 (2019) 5625–5632.
[29] Q.Z. Zhong, S. Li, J. Chen, et al., Angew. Chem. Int. Ed. 58 (2019) 12563–12568.
[30] J. Qin, G. Liang, Y. Feng, et al., Nanoscale 12 (2020) 6096–6103.
[31] G. Yun, Q.A. Besford, S.T. Johnston, et al., Chem. Mater. 30 (2018) 5750–5758.
[32] X. Wang, J. Yan, L. Wang, et al., Chem. Mater. 30 (2018) 4073–4080.
[33] G. Wang, X. Zhou, J. Qin, et al., ACS Appl. Mater. Interfaces 11 (2019) 35060–35067.
[34] X. Cheng, M. Li, H. Wang, Y. Cheng, Chin. Chem. Lett. 31 (2020) 869–874.
[35] H. Pei, Y. Bai, J. Guo, et al., Chin. Chem. Lett. 31 (2020) 505–508.
[36] J.K. Kim, H.A. Lee, H. Lee, H. Chung, Chem. Mater. 30 (2018) 1467–1471.
[37] A. Albanese, P.S. Tang, W.C.W. Chan, Annu. Rev. Biomed. Eng. 14 (2012) 1–16.
[38] Z. Gao, T. Ma, E. Zhao, et al., Small 12 (2016) 556–576.
[39] K.M.L. Taylor, A. Jin, W. Lin, Angew. Chem. Int. Ed. 47 (2008) 7722–7725.
[40] W.J. Rieter, K.M.L. Taylor, H. An, W. Lin, W. Lin, J. Am. Chem. Soc. 128 (2006) 9024–9025.
[41] E. Brücher, in: W. Krause (Ed.), Contrast Agents I: Magnetic Resonance Imaging, Springer Science & Business Media, 2002, pp. 103–122.
[42] P. Caravan, J.J. Ellison, T.J. McMurry, R.B. Lauffer, Chem. Rev. 99 (1999) 2293–2352.
[43] G. Zhao, H. Wu, R. Feng, et al., ACS Appl. Mater. Interfaces 10 (2018) 3295–3304.
[44] J. Wei, G. Wang, F. Chen, et al., Angew. Chem. Int. Ed. 57 (2018) 9838–9843.
[45] X. Wang, J. Yan, D. Pan, et al., Adv. Healthcare Mater. 7 (2018) 1701505.
[46] S. Shen, D. Jiang, L. Cheng, et al., ACS Nano 11 (2017) 9103–9111.
[47] Y. Dai, J. Guo, T.Y. Wang, et al., Adv. Healthcare Mater. 6 (2017) 1700467.
[48] X. Wang, X. Li, X. Liang, et al., J. Mater. Chem. B 6 (2018) 1000–1010.
[49] P.Y. Liu, Z.H. Miao, K. Li, et al., Colloids Surf. B 167 (2018) 183–190.
[50] H. Zhang, Z. Yi, Z. Sun, X. Ma, X. Li, J. Mater. Chem. B 5 (2017) 7622–7631.
[51] F. Liu, X. He, H. Chen, et al., Nat. Commun. 6 (2015) 8003.
[52] D. Raiser, J.J. Deville, Electron Spectrosc. Relat. Phenom. 57 (1991) 91–97.
[53] J. Wei, Y. Hu, Z. Wu, et al., J. Mater. Chem. A 3 (2015) 16867–16873.
[54] H. Xu, J. Nishida, W. Ma, et al., ACS Macro Lett. 1 (2012) 457–460.
[55] Y. Nakano, K. Takeshita, T. Tsutsumi, Water Res. 35 (2001) 496–500.
[56] S. Morisada, Y.H. Kim, T. Ogata, Y. Marutani, Y. Nakano, Ind. Eng. Chem. Res. 50 (2011) 1875–1880.
[57] P. Caravan, Chem. Soc. Rev. 35 (2006) 512–523.
[58] H. Chen, Y. Qiu, D. Ding, et al., Adv. Mater. 30 (2018) 1802748.
[59] J. Bai, X. Jia, W. Zhen, W. Cheng, X. Jiang, J. Am. Chem. Soc. 140 (2018) 106–109.
[60] C. Xu, Y. Wang, H. Yu, H. Tian, X. Chen, ACS Nano 12 (2018) 8255–8265.
[61] K. Yang, J. Wan, S. Zhang, et al., ACS Nano 5 (2011) 516–522.